Available on the CERN CDS information server **CMS PAS HIN-16-002**

CMS Physics Analysis Summary

Contact: cms-pag-conveners-heavyions@cern.ch 2016/09/24

Study of Isolated-Photon + Jet Correlations in PbPb and pp Collisions at $\sqrt{s_{NN}} = 5.02$ TeV

The CMS Collaboration

Abstract

Measurements of correlations in isolated-photon and jet pairs in pp and PbPb collisions at $\sqrt{s_{NN}} = 5.02$ TeV are reported. Jets are reconstructed with an anti-k_{T} clustering algorithm with a distance parameter of 0.3. For events containing a leading isolated photon with transverse momentum $p_{\mathrm{T}}^{\gamma} > 40$ GeV/c and an associated jet with $p_{\mathrm{T}}^{\mathrm{Jet}} > 30$ GeV/c, the photon + jet transverse momentum balance in PbPb collisions is studied as a function of collision centrality and p_{T}^{γ}. The results are compared to pp reference data collected at the same collision energy. A significant decrease in the ratio $p_{\mathrm{T}}^{\mathrm{Jet}}/p_{\mathrm{T}}^{\gamma}$ relative to that in the pp reference is observed.

1 Introduction

Lattice quantum chromodynamics predicts that in relativistic heavy ion collisions, a state of deconfined quarks and gluons known as the Quark-Gluon Plasma (QGP) can be formed [1]. Parton scatterings with large momentum transfer can be used as tomographic probes of the QGP medium, since they are created on very short time scales, $\tau \approx 1/p_{\mathrm{T}} \lesssim 0.1\,\mathrm{fm}/c$, and can potentially lose energy while traversing this medium [2–7].

In lead-lead (PbPb) collisions at the Large Hadron Collider (LHC), a significant transverse momentum (p_{T}) imbalance is observed in back-to-back jets [8, 9]. This imbalance is interpreted as resulting from the in-medium parton energy loss, often referred to as "jet-quenching". In contrast to what is seen in PbPb collisions, no significant dijet p_{T} imbalance is observed in proton-lead collisions [10], which confirms that the observed effect in PbPb collisions does not originate from cold nuclear matter in the initial Pb nucleus.

In the dijet analysis both the leading and the subleading jets are quenched. Transverse momentum asymmetry measurements in the "golden" photon + jet channel have been proposed to be sensitive to the "absolute" in-medium parton energy [11, 12] since photons are not modified when passing through the medium. This assumption is verified by studies of the yields of inclusive isolated photons in PbPb collisions, which are found to match the expectation based on pp data scaled by the number of nucleon-nucleon collisions [13]. At leading order (LO), photons are produced back-to-back with an associated parton (jet) close to the same transverse momentum. Measurements of this kind were first performed in PbPb collisions at $\sqrt{s_{\mathrm{NN}}} = 2.76\,\mathrm{TeV}$ by the CMS collaboration [14]. The precision of this first measurement was limited by the available statistics of the photon + jet pairs.

In 2015, 404 $\mu\mathrm{b}^{-1}$ of PbPb data and 25.8 pb^{-1} of pp data at $\sqrt{s_{\mathrm{NN}}}$ = 5.02 TeV were collected. With these data, high statistics isolated-photon + jet events became available as a result of the increased integrated luminosity, and the larger production cross-section at higher collision energy. The goal of this analysis is to characterize possible modifications of jet properties as a function of centrality and photon p_{T} using isolated-photon+jet events in PbPb collisions. The properties of isolated-photon+jet pairs are studied via the azimuthal angular correlation $\Delta\phi_{\mathrm{J}\gamma} = |\phi^{\mathrm{Jet}} - \phi^{\gamma}|$, the transverse momentum ratio $x_{\mathrm{J}\gamma} = p_{\mathrm{T}}^{\mathrm{Jet}}/p_{\mathrm{T}}^{\gamma}$, and the average number of associated jets per photon, $R_{\mathrm{J}\gamma}$. The results from the PbPb data are compared to those from pp collisions at the same nucleon-nucleon center-of-mass energy to extract information about the modifications due to the presence of the QGP.

2 The CMS detector

Events recorded in pp and PbPb collisions are studied using the CMS detector [15]. The central tracking system is comprised of silicon pixel and strip detectors that allow for the reconstruction of charged-particle trajectories in the pseudorapidity range $|\eta| < 2.5$, where $\eta = -\ln[\tan(\theta/2)]$ and θ is the polar angle relative to the counterclockwise beam direction. It provides an impact parameter resolution of $\approx 15\,\mu\mathrm{m}$ and a p_{T} resolution of about 1.5% for 100 GeV/c particles. Photon candidates used in this analysis are reconstructed using the energy deposited in the barrel region of the $PbWO_4$ crystal electromagnetic calorimeter (ECAL), which covers a pseudorapidity range of $|\eta| < 1.479$, and has a finely segmented granularity of $\Delta\eta \times \Delta\phi = 0.0174 \times 0.0174$. The brass/scintillator hadron calorimeter (HCAL) barrel region covers $|\eta| < 1.74$, and has a segmentation of $\Delta\eta \times \Delta\phi = 0.087 \times 0.087$. Endcap regions of the HCAL and ECAL extend the $|\eta|$ coverage out to about 3. The calorimeters and tracking systems are located within the 3.8 T magnetic field of the super-conducting solenoid. In addition

to the barrel and endcap calorimeters, CMS includes hadron forward (HF) steel/quartz-fibre Cherenkov calorimeters, which cover the forward rapidity of $2.9 < |\eta| < 5.2$ and are used to determine the degree of overlap ("centrality") of the two colliding Pb nuclei [8] in PbPb collisions. An efficient muon system, not used in this analysis, is deployed for the reconstruction and identification of muons up to $|\eta| = 2.4$.

3 Event Selection

Collision events containing high-p_{T} photon candidates are selected online by the CMS trigger system consisting of the Level-1 (L1) and High Level Trigger (HLT). First, events are selected using an inclusive single-photon-candidate L1 trigger with a transverse momentum threshold of 20 (21) GeV/c during the pp (PbPb) data-taking period. Then, photon candidates are reconstructed in the HLT using a clustering algorithm (identical to that used for offline analysis) applied to energy deposits in the ECAL. Events containing a reconstructed photon candidate with $p_{\mathrm{T}}^{\gamma} > 40$ GeV/c are used for further analysis. For minimum-bias PbPb events, the HLT selection efficiency is found to be greater than 98% for events containing a photon with $p_{\mathrm{T}}^{\gamma} > 40$ GeV/c and $|\eta| < 1.44$.

In order to select a pure sample of inelastic hadronic pp and PbPb collisions for analysis, further offline selections are applied to the triggered event sample [8, 16]. Notable among these, a reconstructed event vertex and at least 3 (1) calorimeter towers in the HF on both sides of the interaction point with energy > 3 GeV are required in the PbPb (pp) analysis. Events containing HCAL noise [17] are rejected, to remove possible contamination of the jet sample.

For the analysis of PbPb collisions, the centrality is determined by the total energy from both HF calorimeters. This total energy is used to divide the event sample into centrality bins marked in percentiles of the total inelastic cross section. The most central 30% of the events (i.e., those with smallest impact parameter) are denoted as 0–30%.

4 Photon Reconstruction

Photon candidates are reconstructed from clusters of energy deposited in the ECAL. The algorithms used for the analysis in pp collisions are detailed in Ref. [18], while the optimized clustering algorithm used in high multiplicity PbPb collisions can be found in Ref. [13]. The selected photon candidates used in this analysis are restricted to be in the barrel region of the ECAL by requiring a pseudorapidity limit of $|\eta^{\gamma}| < 1.44$, and are also required to have a transverse momentum of $p_{\mathrm{T}}^{\gamma} > 40$ GeV/c.

In order to remove electron contamination, photon candidates matched with a track within a search window of $|\eta^{\gamma} - \eta^{\mathrm{Track}}| < 0.02$ and $|\phi^{\gamma} - \phi^{\mathrm{Track}}| < 0.15$ are discarded [13]. Anomalous signals caused by the interaction of heavily-ionising particles directly with the silicon avalanche photodiodes used for the ECAL barrel readout are removed, again using the prescription of Ref. [13]. The energy of the reconstructed photons is corrected to account for the effects of the material in front of the ECAL, as well as energy leakage. For the analysis of the PbPb data, an additional correction is applied to account for energy contamination from the PbPb underlying event (UE). The size of the combined energy correction for isolated photons varies from 0 to 10%, depending on the centrality of the collision and the photon p_{T}^{γ}. The corrections are obtained from simulated photon events in PYTHIA embedded into simulated soft background from HYDJET [19, 20].

Since the dominant background for the photon candidates originate from jet fragmentation

with its associated hadrons, a first rejection of neutral mesons mimicking a high-p_{T} photon in the ECAL is done using the ratio of hadronic to electromagnetic energy, H/E. The H/E ratio is defined as the fraction of hadronic energy to the electromagnetic energy inside a cone of $\Delta R = \sqrt{(\Delta\eta)^2 + (\Delta\phi)^2}$ = 0.15 around the photon candidate which is computed from the energy deposition in ECAL and HCAL [21]. Photon candidates with $H/E < 0.1$ are selected for this analysis.

A simulated photon candidate is considered isolated if the sum of the transverse momentum of generated particles in a cone of radius $\Delta R = 0.4$ around the candidate is less than 5 GeV/c. A reconstructed photon candidate is considered isolated if the detector activity in a cone of radius $\Delta R = 0.4$ with respect to the centroid of the cluster, not counting the activity of the cluster and corrected for the underlying event, is less than 1 GeV/c.

The fraction of prompt photons within the collection of candidates (the photon purity) is extracted using a two-component fit of the shape of the electromagnetic shower, discussed in Sec. 6 and further detailed in Ref. [14].

5 Jet Reconstruction

Offline jet reconstruction is performed using the CMS "particle-flow" algorithm [22, 23]. By combining information from all sub-detector systems, the particle-flow algorithm identifies stable particles in an event, classifying them as electrons, muons, photons, charged and neutral hadrons. To form jets, those particle-flow objects are clustered using the anti-k_{T} sequential recombination algorithm provided in the FastJet framework [24, 25]. A small jet radius parameter of $R = 0.3$ is used to minimize the effects of heavy ion background fluctuations in this analysis.

In order to subtract the UE background in PbPb collisions, the iterative algorithm in Ref. [26], using the same implementation as in the PbPb analysis of Ref. [8], is employed. In pp collisions, jets are reconstructed without UE subtraction. The jet energies are corrected to the energies of final-state particle jets using a factorized multi-step approach [27]. The jet energy corrections are derived using simulated PYTHIA events, as well as dijet and photon + jet collision events in pp collisions. Jets with $|\eta| < 1.6$ and corrected $p_{\mathrm{T}} > 30\,\mathrm{GeV}/c$ are selected for final analysis.

6 Analysis

To form photon + jet pairs, the highest p_{T} isolated photon candidate passing the selection criteria and within $|\eta| < 1.44$ in each event is associated with all jets in $|\eta| < 1.6$ in the same event. The combinatorial background in PbPb collisions, including misidentified jets which arise from the UE fluctuation, as well as jets from multiple hard parton-parton scatterings in the same collisions, need to be subtracted in order to study the energy loss effects on the jets produced in the same scattering as the photon. It is estimated by correlating each leading isolated photon candidate to jets found in a different event selected randomly from a set of minimum bias PbPb data in the same centrality class [14].

The background contribution from decay-photon + jet pairs is subtracted from the photon + jet pair sample using a data-driven method. The purity of the photon sample is determined using a template fitting method in the shower shape variable $\sigma_{\eta\eta}$, defined as a modified second moment of the electromagnetic energy cluster distribution around its mean η position:

$$\sigma^2_{\eta\eta} = \frac{\sum_i^{5\times5} w_i(\eta_i - \eta_{5\times5})^2}{\sum_i^{5\times5} w_i}, \qquad w_i = \max(0, 4.7 + \ln\frac{E_i}{E_{5\times5}}), \tag{1}$$

where E_i and η_i are the energy and pseudorapidity of the i^{th} crystal within the 5×5 electromagnetic cluster. $E_{5\times5}$ and $\eta_{5\times5}$ are the total energy and mean η of the 5×5 crystals.

An example of the template fitting method is shown in Fig. 1. The yields and kinematic characteristics of the decay-photon + jet background are estimated by analyzing events with a larger photon shower width ($0.011 < \sigma_{\eta\eta} < 0.017$), which are dominated by background photons from neutral-hadron decays, while the shape of the signal distribution is obtained from PYTHIA+HYDJET simulations in each centrality class. The estimated background contribution fraction (1 − photon purity) is then subtracted from the yield for the signal events, which have a smaller photon shower width ($\sigma_{\eta\eta} < 0.010$).

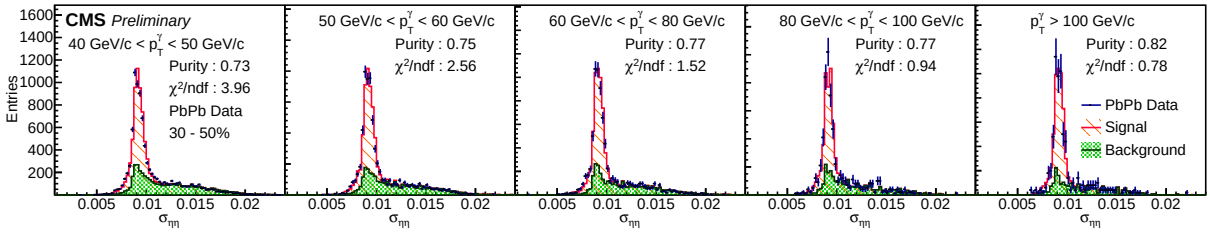

Figure 1: The shower shape variable ($\sigma_{\eta\eta}$) of photons from mid-central (30-50%) PbPb collisions. The black points are PbPb data, the red histogram is the signal template from PYTHIA+HYDJET, and the green histogram is the background template from a non-isolated data sideband. The purity is defined as the fraction of isolated photons in the signal region $\sigma_{\eta\eta} < 0.01$ used in the isolated-photon + jet analysis.

In order to compare PbPb collisions with the pp reference, the jet energy in pp events is smeared to match the jet energy resolution in each of the PbPb centrality classes. The jet energy resolution is calculated from Gaussian fits to the ratio of reconstructed jet p_{T} to generated jet p_{T} in PYTHIA+HYDJET for PbPb and PYTHIA for pp, and the difference in resolution between pp and PbPb is used to smear the pp data.

The systematic uncertainties are estimated for each observable using similar procedure as described in Ref. [14]. The total uncertainties are calculated by summing in quadrature of the uncertainties from various sources: (a) photon purity (b) photon energy scale (c) electron contamination (d) photon isolation criteria (e) jet energy resolution and (f) jet energy scale. A summary of the average systematic uncertainties for $\sigma(\Delta\phi_{\mathrm{J}\gamma})$, which is the width of an exponential fit to the $\Delta\phi_{\mathrm{J}\gamma}$ distribution, $R_{\mathrm{J}\gamma}$, and $\langle x_{\mathrm{J}\gamma}\rangle$ in PbPb collisions is shown in Table 1.

7 Results

7.1 Photon + jet azimuthal correlation

Possible medium modification of the back-to-back photon and recoiling jet aligment can be studied by comparing the relative azimuthal angle ($\Delta\phi_{\mathrm{J}\gamma}$) distributions in pp and PbPb collisions. The shape of the $\Delta\phi_{\mathrm{J}\gamma}$ distribution in PbPb collisions is studied in bins of leading photon p_{T} and two event centrality intervals, and it is shown in Fig. 2. Within the quoted statistical uncertainty, the results in pp and PbPb collisions are consistent with each other.

Systematic Uncertainty	$\langle x_{J\gamma} \rangle$ $p_T^\gamma > 60$ GeV/c	$\langle x_{J\gamma} \rangle$ 0-30%	$\langle x_{J\gamma} \rangle$ 30-100%	$\sigma(\Delta\phi_{J\gamma})$ $p_T^\gamma > 60$ GeV/c
Photon Purity	2.9%	3.3%	1.9%	1.6%
Photon Energy Scale	0.7%	0.6%	0.5%	2.4%
Electron Contamination	<0.5%	<0.5%	<0.5%	0.9%
Photon Isolation	0.9%	0.7%	0.6%	3.6%
Jet Energy Resolution	2.6%	3.8%	2.1%	2.4%
Jet Energy Scale	3.8%	3.3%	3.6%	4.8%

Systematic Uncertainty	$R_{J\gamma}$ $p_T^\gamma > 60$ GeV	$R_{J\gamma}$ 0-30%	$R_{J\gamma}$ 30-100%
Photon Purity	1.3%	3.3%	2.5%
Photon Energy Scale	0.6%	<0.5%	0.8%
Electron Contamination	0.6%	<0.5%	0.6%
Photon Isolation	0.7%	1.7%	0.8%
Jet Energy Resolution	4.8%	7.7%	4.9%
Jet Energy Scale	5.6%	8.4%	6.1%

Table 1: Summary of the average systematic uncertainties. Columns which do not specify the p_T^γ cut have a cut of $p_T^\gamma > 40$. Columns which do not specify the centrality bin are centrality-inclusive.

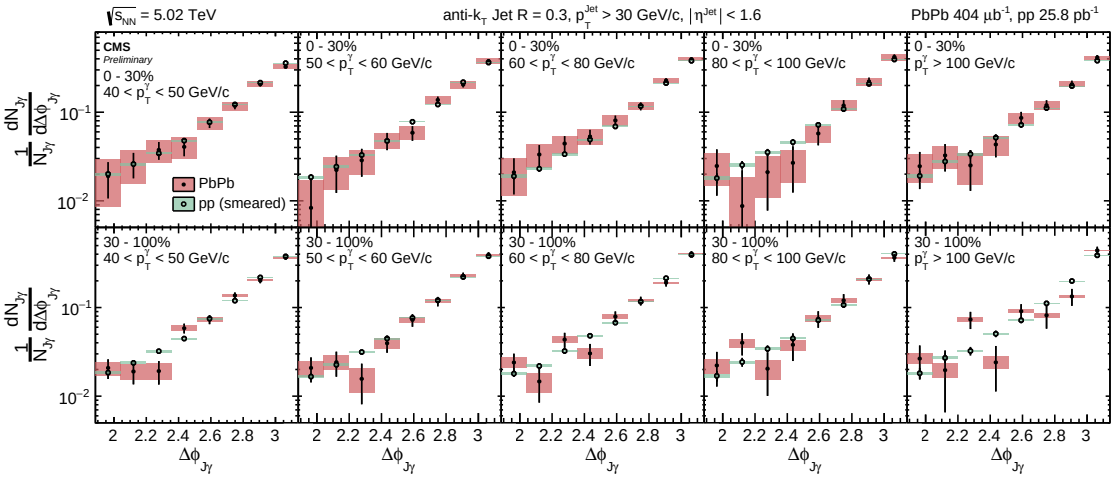

Figure 2: Azimuthal correlation of photons and jets in each p_T^γ bin (from left to right) for central PbPb (top) and peripheral PbPb (bottom) after mixed event background subtraction. The correlation is shown on a logarithmic scale and its range is restricted to $\Delta\phi_{J\gamma} > \frac{3\pi}{5}$. The PbPb data is compared to smeared pp data. The lines through the points represent the statistical uncertainty while the shaded boxes represent the systematic uncertainty.

7.2 Photon + jet transverse momentum imbalance

The asymmetry ratio $x_{J\gamma} = p_T^{Jet}/p_T^{\gamma}$ is used to quantify the photon + jet transverse momentum imbalance. In addition to the photon and jet selections used in the $\Delta\phi_{J\gamma}$ study, a strict $\Delta\phi_{J\gamma} > \frac{7}{8}\pi$ selection is applied to suppress contribution from background jets as well as photon+2-jets events. Figure 3 shows the normalized $x_{J\gamma}$ distributions for different centrality and p_T^{γ} regions in pp and PbPb collisions. The pp data is smeared to account for the jet resolution difference in pp and PbPb collisions when compared with PbPb data. A significant modification with respect to the smeared pp reference is observed in 0–30% PbPb collisions. The mean of the $x_{J\gamma}$ as a function of photon p_T is shown in Fig. 4. In the region $p_T^{\gamma} < 60$ GeV/c, the $\langle x_{J\gamma} \rangle$ in smeared pp and PbPb collisions are consistent within the quoted uncertainty.

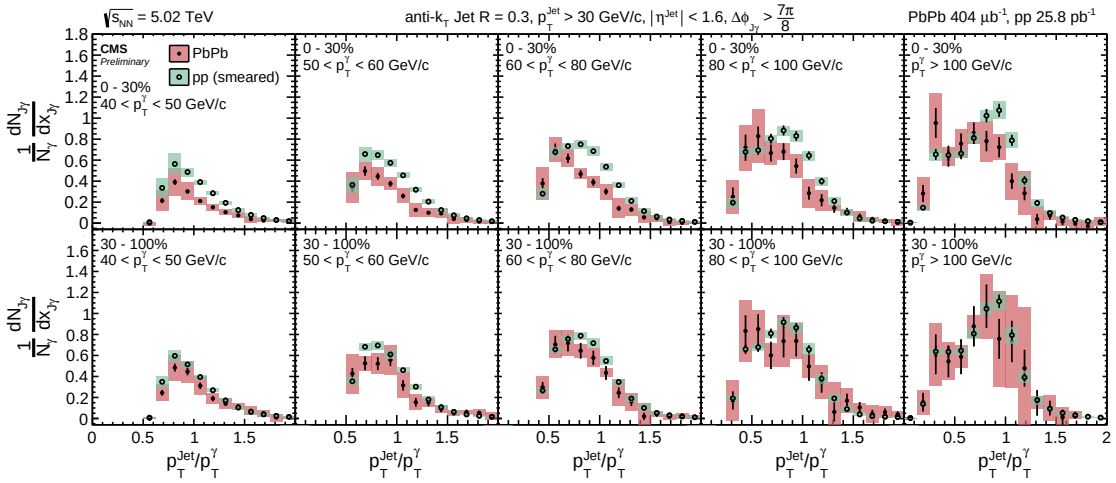

Figure 3: Distribution of $x_{J\gamma} = p_T^{Jet}/p_T^{\gamma}$ in each p_T^{γ} bin (from left to right) for central PbPb (top) and peripheral PbPb (bottom). The PbPb data are compared to smeared pp data. The lines through the points represent the statistical uncertainty while the shaded boxes represent the systematic uncertainty.

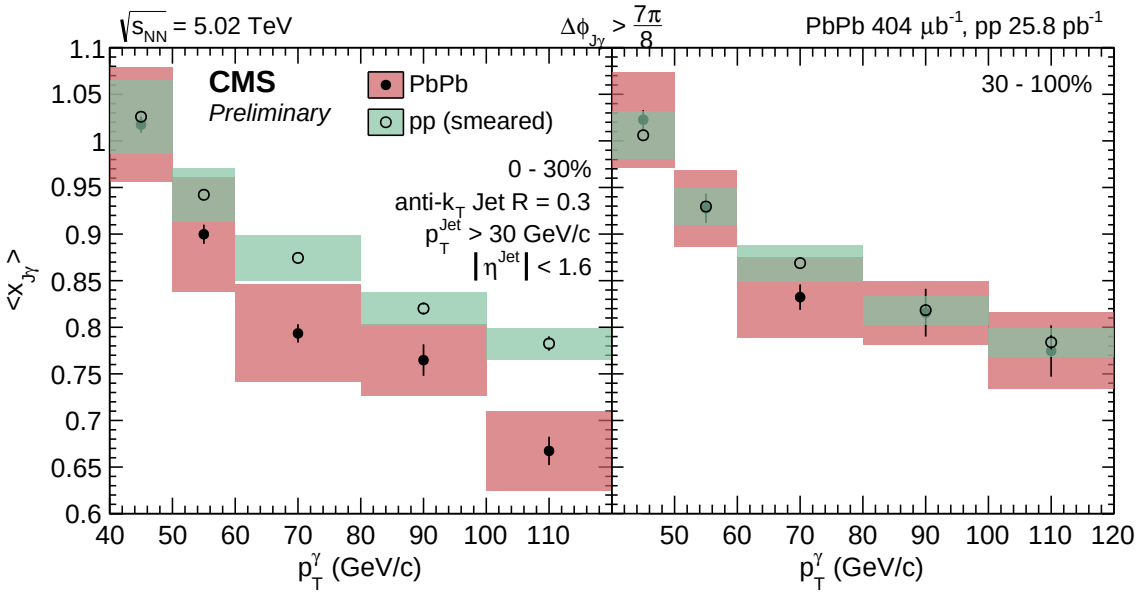

Figure 4: Average jet over photon transverse momentum ratio ($\langle x_{J\gamma} \rangle$) of the recoiled jets in (left) smeared pp and central PbPb, and (right) smeared pp and peripheral PbPb. The pp results are smeared by the relative jet energy resolution in order to account for the underlying event fluctuations when compared to PbPb data. The lines through the points represent the statistical uncertainty while the shaded boxes represent the systematic uncertainty.

7.3 Average Number of Associated Jets per Photon

With a jet p_T threshold of 30 GeV/c, the average energy imbalance of the selected photon + jet pairs does not constitute a full picture. There are photon + jet pairs that do not contribute to the $\langle x_{J\gamma} \rangle$ because the associated jets fall below this threshold. To quantify the effect, the average number of associated jets per photon passing the analysis selection ($R_{J\gamma}$) is shown in Fig. 5. In the 0–30% central PbPb collisions, the value of $R_{J\gamma}$ is found to be lower than the smeared pp data in all leading photon p_T bins.

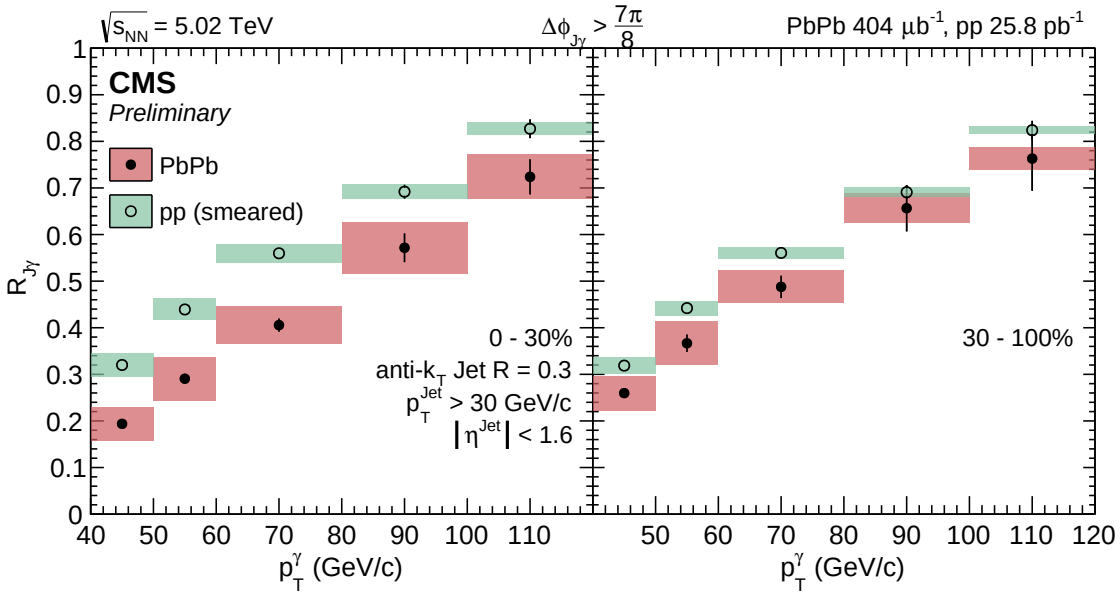

Figure 5: Average number of associated jets per photon ($R_{J\gamma}$) as a function of leading photon p_T in (left) smeared pp and central PbPb, and (right) smeared pp and peripheral PbPb. The jet energy in the pp data is smeared by the relative jet energy resolution in order to account for the underlying event fluctuations when compared to PbPb data. The lines through the points represent the statistical uncertainty while the shaded boxes represent the systematic uncertainty.

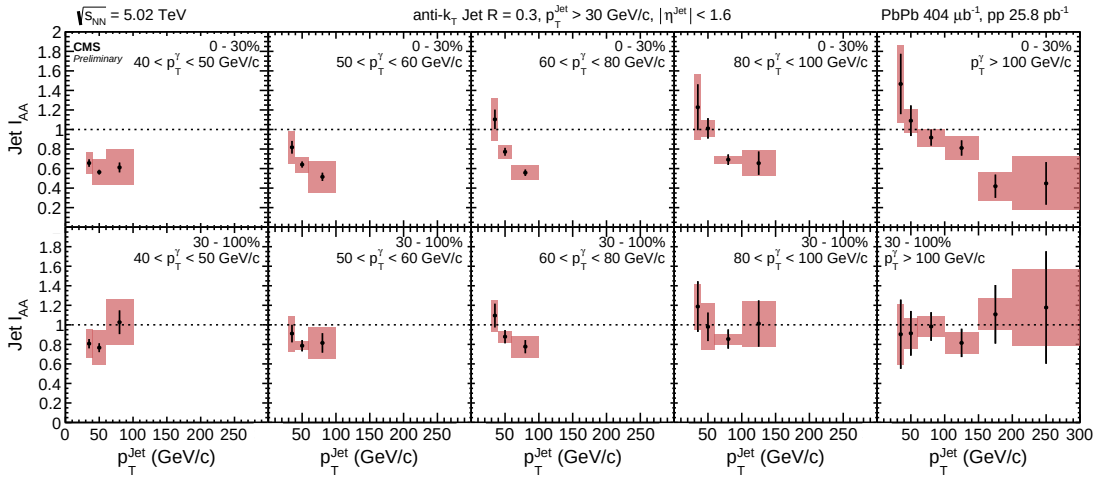

Figure 6: Ratio of jet yield in PbPb collisions to smeared pp. In the low p_{T}^{γ} events, the yields in central PbPb events are smaller than in pp for all $p_{\mathrm{T}}^{\mathrm{Jet}}$ bins. As p_{T}^{γ} increases, yields at low $p_{\mathrm{T}}^{\mathrm{Jet}}$ are greater in PbPb than smeared pp. The lines through the points represent the statistical uncertainty while the shaded boxes represent the systematic uncertainty.

7.4 Jet yield ratio

In order to illustrate the medium modification of the associated jet p_{T} spectra, the ratio of the associated jet yields in PbPb and smeared pp events, $\mathrm{I_{AA}}$, is shown in Fig. 6. In central PbPb events, the associated yield is suppressed by a factor of two in low p_{T}^{γ} bins. As p_{T}^{γ} increases, an excess of jets appears at low $p_{\mathrm{T}}^{\mathrm{Jet}}$ in central PbPb as the increased phase space at high p_{T}^{γ} allows the quenched jets to remain above the kinematic cuts.

7.5 Centrality Dependence

The centrality dependence of $x_{\mathrm{J}\gamma}$ for PbPb collisions with $p_{\mathrm{T}}^{\gamma} > 60$ GeV/c is shown in Fig. 7. When compared to the smeared pp data, the PbPb collision data exhibit a change in shape, shifting the distribution towards lower $x_{\mathrm{J}\gamma}$ as the collisions become more central.

The following figures are shown as a function of the average number of participants estimated from a Monte Carlo Glauber model and weighted by the number of collisions to account for the hard scattering bias within each centrality bin.

To study the centrality evolution of the $\Delta\phi_{\mathrm{J}\gamma}$ shape in PbPb collisions, the distributions are fitted to an exponential function:

$$\frac{1}{N_{J\gamma}}\frac{dN_{J\gamma}}{d\Delta\phi_{\mathrm{J}\gamma}} = A + Be^{\frac{\Delta\phi-\pi}{\sigma}} \tag{2}$$

where A is constant pedestal and σ is the width of the distribution. The fit is restricted to the exponentially falling region $\Delta\phi > 2\pi/3$. The results obtained from PbPb collisions and smeared pp data are consistent with each other as shown in Fig. 8.

Figures 9 and 10 show the results $R_{\mathrm{J}\gamma}$ and $\langle x_{\mathrm{J}\gamma}\rangle$ in pp and PbPb collisions as a function of event centrality. In central collisions, a reduction in $R_{\mathrm{J}\gamma}$ and $\langle x_{\mathrm{J}\gamma}\rangle$ is observed in comparison to the

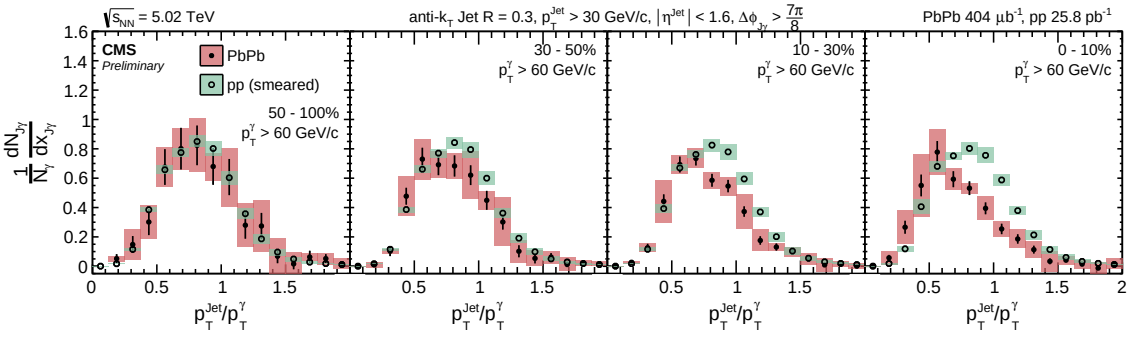

Figure 7: Distribution of $x_{J\gamma}$ of photon+jet pairs of pp and PbPb collisions normalized by the number of photon+jet pairs. The momenta of jets in pp are smeared by the relative jet energy resolution to be used as the reference of each centrality bin. The lines through the points represent the statistical uncertainty while the shaded boxes represent the systematic uncertainty.

pp reference, confirming the observation of away-side jet energy loss.

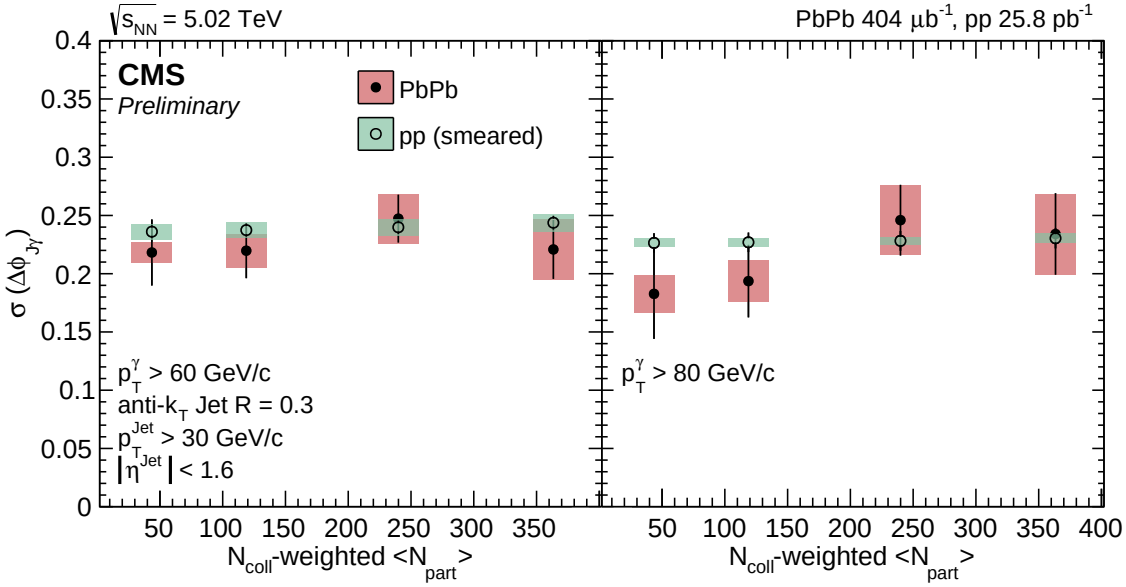

Figure 8: Comparison of $\Delta\phi_{J\gamma}$ width in pp and PbPb collisions shown for different $p_{\mathrm{T}}^{\mathrm{Jet}}$ bins as a function of the average number of participants weighted by the number of collisions. The momenta of jets in pp are smeared by the relative jet energy resolution to be used as the reference of each centrality bin. The lines through the points represent the statistical uncertainty while the shaded boxes represent the systematic uncertainty.

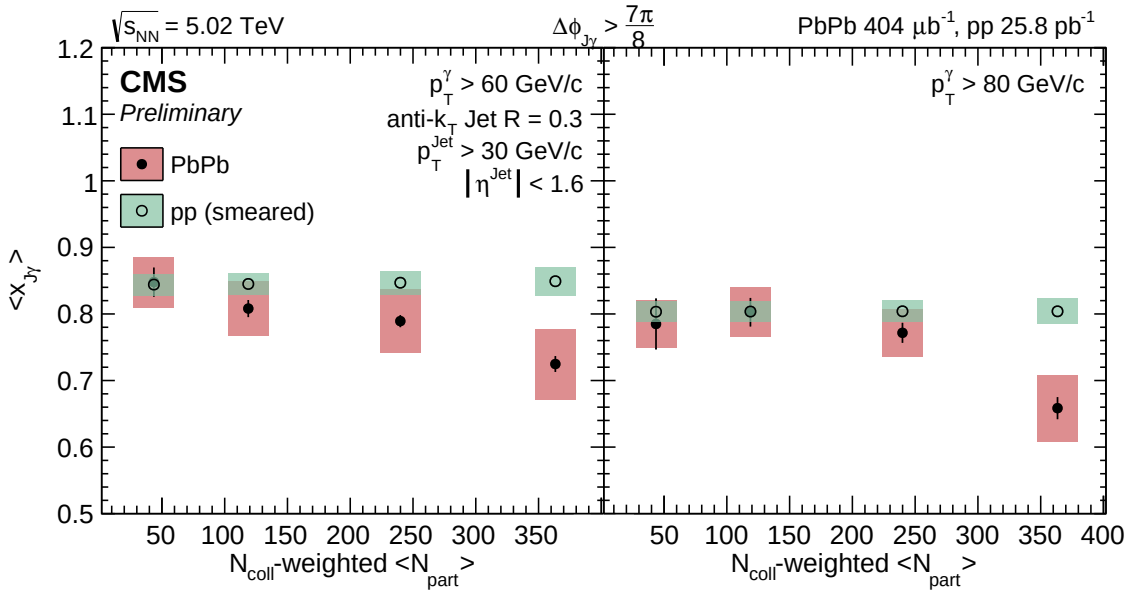

Figure 9: Comparison of $\langle x_{J\gamma} \rangle$ in pp and PbPb collisions as a function of the average number of participants weighted by the number of collisions. The momenta of jets in pp are smeared by the relative jet energy resolution to be used as the reference of each centrality bin. The lines through the points represent the statistical uncertainty while the shaded boxes represent the systematic uncertainty.

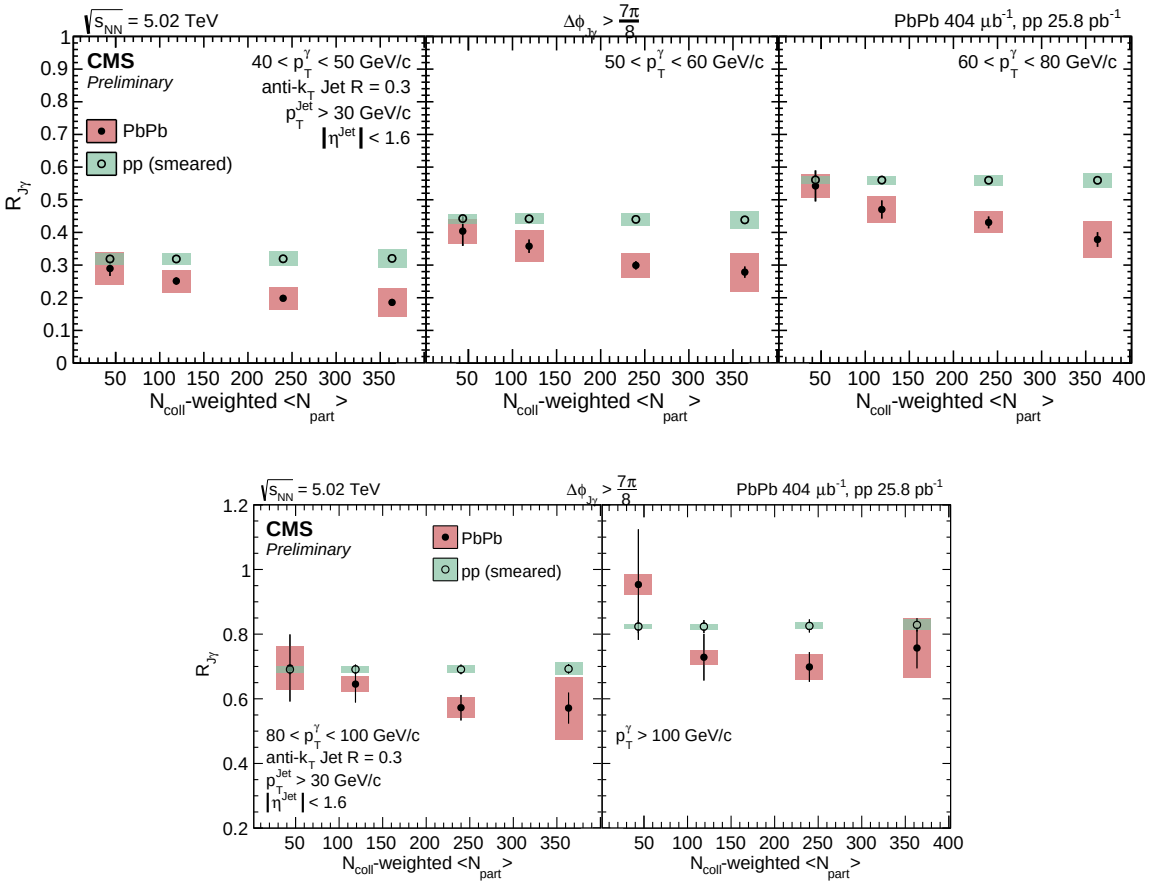

Figure 10: Comparison of $R_{J\gamma}$ in pp and PbPb collisions as a function of the average number of participants weighted by the number of collisions. The momenta of jets in pp are smeared by the relative jet energy resolution to be used as the reference of each centrality bin. The lines through the points represent the statistical uncertainty while the shaded boxes represent the systematic uncertainty.

8 Summary

Studies of isolated-photon + jet correlations in pp and PbPb at $\sqrt{s_{NN}} = 5.02$ TeV are reported. The photon + jet transverse momentum ratio, $x_{J\gamma} = p_T^{Jet}/p_T^{\gamma}$, and the fraction of photons with an associated jet, $R_{J\gamma}$, are studied in bins of leading photon p_T and PbPb collision centrality. For all p_T^{γ} bins, $\langle x_{J\gamma} \rangle$ and $R_{J\gamma}$ in the 0–30% central PbPb collisions are found to be lower than corresponding pp reference values, indicating that a larger fraction of jets lose energy and fall below 30 GeV/c in the PbPb system. By comparing the yields of jets in PbPb and pp collisions triggered by photons above 80 GeV/c, a shift of the jet spectra toward the lower p_T^{Jet} direction is observed.

References

[1] F. Karsch, "The Phase transition to the quark gluon plasma: Recent results from lattice calculations", *Nucl. Phys. A* **590** (1995) 367C–382C, doi:10.1016/0375-9474(95)00248-Y, arXiv:hep-lat/9503010.

[2] D. A. Appel, "Jets as a probe of quark-gluon plasmas", *Phys. Rev.* **D33** (1986) 717, doi:10.1103/PhysRevD.33.717.

[3] J. Blaizot and L. D. McLerran, "Jets in Expanding Quark - Gluon Plasmas", *Phys. Rev. D* **34** (1986) 2739, doi:10.1103/PhysRevD.34.2739.

[4] M. Gyulassy and M. Plumer, "Jet Quenching in Dense Matter", *Phys. Lett. B* **243** (1990) 432–438, doi:10.1016/0370-2693(90)91409-5.

[5] X.-N. Wang and M. Gyulassy, "Gluon shadowing and jet quenching in A + A collisions at $\sqrt{s} = 200A$ GeV", *Phys. Rev. Lett.* **68** (1992) 1480–1483, doi:10.1103/PhysRevLett.68.1480.

[6] R. Baier et al., "Radiative energy loss and p(T) broadening of high-energy partons in nuclei", *Nucl. Phys. B* **484** (1997) 265–282, doi:10.1016/S0550-3213(96)00581-0, arXiv:hep-ph/9608322.

[7] B. Zakharov, "Radiative energy loss of high-energy quarks in finite size nuclear matter and quark - gluon plasma", *JETP Lett.* **65** (1997) 615–620, doi:10.1134/1.567389, arXiv:hep-ph/9704255.

[8] CMS Collaboration, "Observation and studies of jet quenching in PbPb collisions at nucleon-nucleon center-of-mass energy = 2.76 TeV", *Phys. Rev. C* **84** (2011) 024906, doi:10.1103/PhysRevC.84.024906, arXiv:1102.1957.

[9] ATLAS Collaboration, "Observation of a Centrality-Dependent Dijet Asymmetry in Lead-Lead Collisions at $\sqrt{S_{NN}} = 2.76$ TeV with the ATLAS Detector at the LHC", *Phys. Rev. Lett.* **105** (2010) 252303, doi:10.1103/PhysRevLett.105.252303, arXiv:1011.6182.

[10] CMS Collaboration, "Studies of dijet transverse momentum balance and pseudorapidity distributions in pPb collisions at $\sqrt{s_{NN}} = 5.02$ TeV", *Eur. Phys. J. C* **74** (2014) 2951, doi:10.1140/epjc/s10052-014-2951-y, arXiv:1401.4433.

[11] X.-N. Wang, Z. Huang, and I. Sarcevic, "Jet Quenching in the Direction Opposite to a Tagged Photon in High-Energy Heavy-Ion Collisions", *Phys. Rev. Lett.* **77** (1996) 231–234, doi:10.1103/PhysRevLett.77.231.

[12] X.-N. Wang and Z. Huang, "Medium-induced parton energy loss in γ+jet events of high-energy heavy-ion collisions", *Phys. Rev. C* **55** (1997) 3047–3061, doi:10.1103/PhysRevC.55.3047.

[13] CMS Collaboration, "Measurement of isolated photon production in pp and PbPb collisions at $\sqrt{s_{NN}} = 2.76$ TeV", *Phys. Lett. B* **710** (2012) 256–277, doi:10.1016/j.physletb.2012.02.077, arXiv:1201.3093.

[14] CMS Collaboration, "Studies of jet quenching using isolated-photon+jet correlations in PbPb and pp collisions at $\sqrt{s_{NN}} = 2.76$ TeV", *Phys. Lett. B* **718** (2013) 773–794, doi:10.1016/j.physletb.2012.11.003, arXiv:1205.0206.

[15] CMS Collaboration, "The CMS experiment at the CERN LHC", *JINST* **03** (2008) S08004, doi:10.1088/1748-0221/3/08/S08004.

[16] CMS Collaboration, "Transverse-momentum and pseudorapidity distributions of charged hadrons in pp collisions at $\sqrt{s} = 7$ TeV", *Phys. Rev. Lett.* **105** (2010) 022002, doi:10.1103/PhysRevLett.105.022002, arXiv:1005.3299.

[17] CMS Collaboration, "Identification and Filtering of Uncharacteristic Noise in the CMS Hadron Calorimeter", *JINST* **5** (2010) T03014, doi:10.1088/1748-0221/5/03/T03014, arXiv:0911.4881.

[18] CMS Collaboration, "Performance of photon reconstruction and identification with the CMS detector in proton-proton collisions at $\sqrt{s} = 8$ TeV", *Journal of Instrumentation* **10** (2015) doi:10.1088/1748-0221/10/08/P08010, arXiv:1502.02702.

[19] T. Sjöstrand, S. Mrenna, and P. Z. Skands, "A brief introduction to PYTHIA 8.1", *Comput. Phys. Commun.* **178** (2008) 852, doi:10.1016/j.cpc.2008.01.036, arXiv:0710.3820.

[20] I. P. Lokhtin and A. M. Snigirev, "A model of jet quenching in ultrarelativistic heavy ion collisions and high-pT hadron spectra at RHIC", *Eur. Phys. J.* **C45** (2006) 211, doi:10.1140/epjc/s2005-02426-3, arXiv:hep-ph/0506189.

[21] CMS Collaboration, "Measurement of the Isolated Prompt Photon Production Cross Section in pp Collisions at $\sqrt{s} = 7$ TeV", *Phys. Rev. Lett.* **106** (2011) 082001, doi:10.1103/PhysRevLett.106.082001, arXiv:1012.0799.

[22] CMS Collaboration, "Particle–Flow Event Reconstruction in CMS and Performance for Jets, Taus, and $E_{\mathrm{T}}^{\mathrm{miss}}$", *CMS Physics Analysis Summary* **CMS-PAS-PFT-09-001** (2009).

[23] CMS Collaboration, "Commissioning of the Particle-flow Event Reconstruction with the first LHC collisions recorded in the CMS detector", *CMS Physics Analysis Summary* **CMS-PAS-PFT-10-001** (2010).

[24] M. Cacciari, G. P. Salam, and G. Soyez, "The Anti-k(t) jet clustering algorithm", *JHEP* **0804** (2008) 063, doi:10.1088/1126-6708/2008/04/063, arXiv:0802.1189.

[25] M. Cacciari, G. P. Salam, and G. Soyez, "FastJet User Manual", *Eur. Phys. J. C* **72** (2012) 1896, doi:10.1140/epjc/s10052-012-1896-2, arXiv:1111.6097.

[26] O. Kodolova, I. Vardanian, A. Nikitenko, and A. Oulianov, "The performance of the jet identification and reconstruction in heavy ions collisions with CMS detector", *Eur. Phys. J.* **C50** (2007) 117, doi:10.1140/epjc/s10052-007-0223-9.

[27] CMS Collaboration, "Determination of Jet Energy Calibration and Transverse Momentum Resolution in CMS", *JINST* **6** (2011) P11002, doi:10.1088/1748-0221/6/11/P11002, arXiv:1107.4277.